Development of Ni–Al$_2$SiO$_5$/Ni–SiO$_2$ Coating Doped with Benzotriazole: Corrosion, Structural Evolution and Thermal Degradation Study

G. Akande[1*], O. S. I. Fayomi [1], A. P. I. Popoola[3], T. Daantjie[3], O. O. Oluwole [2] and B. O. Olatunji[4]

[1]*Department of Mechanical Engineering, Bells University of Technology, P.O. Box 1015, Ota, Ogun State, Nigeria*
[2]*Department of Mechanical Engineering, University of Ibadan, Ibadan, Oyo State, Nigeria*
[3]*Department of Chemical, Metallurgical and Materials Engineering, Tshwane University of Technology, P.O. Box 680, Pretoria, South Africa*
[4]*Prototype Engineering Development Institute, PEDI, Ilesha, Osun State, Nigeria*
Corresponding author. aigodwin2015@gmail.com

Abstract

Several engineering mild steel components have catastrophically failed, due to structural defects, corrosion and wear deformation. These drawbacks have prompted a continuous mild steel modification, for its higher durability and efficiency. In an attempt to improve the metal performance, Ni–SiO$_2$ (silicon dioxide), Ni–SiO$_2$–C$_6$H$_5$N$_3$ (1H-benzotriazole), Ni–Al$_2$SiO$_5$ (niquel + aluminum silicate) and Ni–Al$_2$SiO$_5$–10C$_6$H$_5$N$_3$ composite films were developed on mild steel samples, at a constant temperature of 45 ºC, and deposition time of 20 min. The coating performances were investigated by potentiodynamic polarization technique, CERT UMT-2 multi-functional tribological testing, high resolution optical microscopy and high diamond pyramid indentation. The samples were further subjected to heat treatment, and its effects on hardness were examined. Potentiodynamic polarization study carried out in 0.5 M HCl revealed an improved anti-corrosion resistance. The hardness and wear tests showed better mild steel mechanical properties. Ni– Al$_2$SiO$_5$–10C$_6$H$_5$N$_3$ coated sample had better hardness and wear resistance features that those from the other samples. High resolution optical microscopy unveiled the particles homogeneous distribution throughout mild steel, with a new surface evolution. Mild steel surface morphology and other properties was optimized by Ni–SiO$_2$, Ni–SiO$_2$–C$_6$H$_5$N$_3$, Ni–Al$_2$SiO$_5$ and Ni–Al$_2$SiO$_5$–10C$_6$H$_5$N$_3$ coatings. Comparatively, NiAl$_2$SiO$_5$– C$_6$H$_5$N$_3$ coated mild steel exhibited the overall best performance characteristics, and it is thus recommended for advanced applications in petrochemical and marine industries.

Keywords: wear, corrosion, mild steel, hardness and polarization.

Introduction

Corrosion, wear and fracture are some of the main damage suffered by mild steel, which has resulted in its components degradation and lower durability. These have

been major concerns in various industrial set-ups [1-3]. Surface modifications via composite coatings have been widely utilized to improve mild steel properties for advanced and sophisticated applications [4, 5]. The preference for mild steel coating through electrodeposition technique over other surface modification methods is due to its bonding efficiency, cost effectiveness, fine texture and good thickness ratio [6]. Cobalt (Co), Ni and Zinc (Zn) mono coatings have been used to be deposited on mild steel [7]. However, multiple failures were reported, due to their low durability in high corrosive and intensely abrasive environments [8-10]. These challenges have been addressed by employing composite deposition as an alternative for improving the mono coatings properties [11-13].

Steel surface coating with particles from the oxidation of metals, ceramic and polymers has effectively provided substantial tribological properties and good oxidation stability [14-17]. Electrodeposition of composites, such as ZnO (zinc oxide), Al_2O_3 (aluminum oxide), Cr_2O_3 (chromium oxide), TiO_2 (titanium dioxide), Al_6O_{13}, SiC (silicon carbid), WC (tungsten carbide) and Cr_3C_2 (chromium carbide), have proved effective to a certain degree [18, 19]. However, the search for better materials, to obtain mechanical, tribological, corrosion resistance and surface morphology optimization, continues [20-22]. Improved metals surface morphology has been achieved by ensuring the particles homogenous distribution through their continued agitation, to avoid their agglomeration. Other processing parameters might as well affect the metals coating morphology [23]. This work has investigated the effect of $Ni–SiO_2$, $Ni–SiO_2–C_6H_5N_3$, $Ni–Al_2SiO_5$ and $Ni–Al_2SiO_5–10C_6H_5N_3$ composite films on mild steel corrosion resistance in a 0.5 M HCl solution, via linear potentiodynamic polarization technique. The samples micro-hardness, wear resistance and surface morphologies were investigated to establish their performance.

Experimental procedure substrates preparation

Mild steel commercially sourced was cut into coupons, with the dimensions of 45 mm x 25 mm x 2mm, and used as cathode, while a 99% Ni plate, with the dimensions of 50 mm x 30 mm x 2 mm, was the anode. The mild steel samples surfaces were cleaned with emery papers, and submerged in sodium carbonate for 10 s, to remove rusty particles from them. The mild steel samples were then pickled and activated with 10% HCl, at room temperature, for 10 s. The pickled mild steel samples were instantly rinsed in distilled water. The mild steel chemical composition used for this experiment is shown in Table 1.

Table 1. Mild steel composition (wt%).

Element	C	Mn	Si	P	S	Al	Ni	Fe
Composition	0.15	0.452	0.181	0.011	0.0312	0.0051	0.007	Balance

Coating bath preparation

Table 2 shows the bath formulation for $Ni–30SiO_2$ and $Ni–30SiO_2–10C_6H_5N_3$ coating, while Table 3 shows the bath formulation for $Ni–30Al_2SiO_5$ and $Ni–30Al_2SiO_5–20C_6H_5N_3$ coating. The reagents and particles were dissolved in

distilled water, and left for 48 h, maintaining a constant pH value, and temperatures of 5.0 and 45 ºC, respectively.

Table 2. Composition and operating conditions for silica (SiO_2) baths.

Composition	Mass concentration (g/L)
$NiSO_4$	70
SiO_2	30
$C_6H_5N_3$	0 and 10
Na_2SO_4	15
Thiourea	5
Boric acid	15
Glycine	5
Operating conditions	
pH	5.0
Cell voltage	0.5 V
Time	20 min.
Temp.	45 ºC

Table 3. Composition and operating conditions for Al_2SiO_5 baths.

Composition	Mass concentration (g/L)
$NiSO_4$	70
Al_2SiO_5	30
$C_6H_5N_3$	0 and 10
Na_2SO_4	15
Thiourea	5
Boric acid	15
Glycine	5
Operating conditions	
pH	0,5
Cell voltage	0.5 V
Time	20 min.
Temp.	45 ºC

Electrodeposition process

During the electrodeposition process, mild steel was positioned at an equivalent distance of 3 cm between two nickel plates. The plating bath was continuously stirred at 250 rpm, and a constant temperature of 45 ºC was maintained throughout the coating process. The constant stirring ensured the particles stable suspension, and reduced their sticking tendency. The charge particle electrophoresis mobility in the solution was enhanced, due to the minimal particles agglomeration [24]. Constant agitation aided the particles mass transfer, and also enhanced deposition quality. However, inordinate agitation could be detrimental to the electrodes stability, affecting the charge transfer region and, consequently, reducing the deposition quality [25].

Samples characterization

The coated samples thicknesses were measured using an Elcometer microthickness meter gauge (Elcometer 456 Model). with the accuracy of ±1%. The uncoated and coated samples corrosion resistances were examined using a potentiodynamic polarization technique that utilizes a three-electrode cell system in 0.5 M HCl, at

an ambient temperature of 25 °C. The contact and reference electrode were the graphite rod and Ag/AgCl, respectively. Tafel curves were generated from -1.5 to 1.5 V, at a 0.005 V/s scan rate. The test samples wear and hardness were investigated using a CERT UMT-2 multi-functional tribological testing and a high diamond pyramid indentation, respectively. The samples wear characterizations were carried out at a room temperature of 25 °C, using a load of 10 N, at a constant speed of 5 mm/s and a displacement amplitude of 2 mm, for 20 min, on the reciprocating sliding tester. A silicon nitride (Si_3N_4) ball, with the diameter of 4 mm and mass of 50 g, was used as the counter body, for examining the sample wear behavior. More so, the test samples morphologies were examined using a high resolution optical microscopy, at 10 X magnification. The test samples heattreatment was carried out in a vacuum, at 400 °C, for 1 h.

Results and discussion
Coating thickness and estimation of coating per unit area
Table 4 shows the average thickness obtained from the samples thickness measurement at different points. The coating per unit area (mg/mm^2) was calculated using equation 1 or 2.

$$Ca = \frac{W}{2(LT + LB + BT)} \qquad (1)$$

$$Ca = \frac{W}{A} \qquad (2)$$

where w, L, T and B are the samples weight gain, length, thickness and breadth, respectively, and A is their coated area.

Table 4. Thickness and weight gained by the coated samples.

| Coated sample	Coating thickness (μm)	Weight gain (g)	Coating per unit area (mg/mm²)
Ni–30SiO₂	134.3	0.16	0.063241
Ni–30SiO₂–10C₆H₅N₃	156.7	0.28	0.110672
Ni–30Al₂SiO₅	152.1	0.26	0.102768
Ni–30Al₂SiO₅–10C₆H₅N₃	177.5	0.31	0.122523

Linear potentiodynamic polarization
The coated test samples linear potentiodynamic polarization examination showed that they had lower corrosion resistance, in the 0.5 M HCl solution, than that of the control sample. Table 5 and Fig. 1 show the summary of the potentiodynamic polarization results and the Tafel plot, respectively.
In Table 5, it can be seen that the Ni–30SiO₂–10C₆H₅N₃ coated sample exhibited a lower corrosion rate (E_{corr}) that that of the Ni–30SiO₂ coated sample. Similarly, the Ni–30Al₂SiO₅–10C₆H₅N₃ coated sample was found to possess a lower E_{corr} than that of the Ni–30Al₂SiO₅ coated samples. This shows that the 1H-benzotriazole (10C₆H₅N₃) addition further hindered the mild steel active sites attack by the Cl⁻ ion.

Table 5. Potentiodynamic polarization results.

Sample	E_{corr} (V)	j_{corr} (A/cm^2)	R_p (Ω)	Cr (mm/yr)
Control	-0.4952	3.12E-04	183.17	2.8979
Ni–30SiO$_2$	-0.3730	2.05E-04	295.71	1.2186
Ni–30SiO$_2$–10C$_6$H$_5$N$_3$	-0.3694	1.13E-04	447.36	1.1028
Ni–30Al$_2$SiO$_5$	-0.4859	5.57E-05	620.43	0.5121
Ni–30Al$_2$SiO$_5$–10C$_6$H$_5$N$_3$	-0.3738	4.14E-05	622.46	0.4470
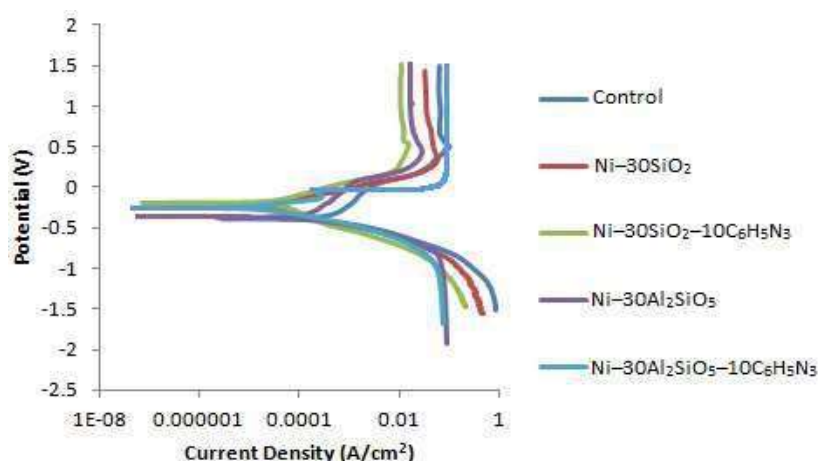
Figure 1. Tafel plots of the test samples.

More so, the lowest current density (j_{corr}) and highest degree of polarization resistance (R_p), recorded for the Ni–30Al$_2$SiO$_5$–10C$_6$H$_5$N$_3$ coated sample, could be attributed to the synergetic effect of both Al$_2$SiO$_5$ and 10C$_6$H$_5$N$_3$, and to their adhesiveness on mild steel [26]. The Tafel plot in Fig. 1 revealed the particulates mixed inhibitory effect. This was confirmed by the E_{corr} values closeness.

Samples microhardness analysis
Fig. 2 shows the micro-hardness values of heat-treated and unheated samples.
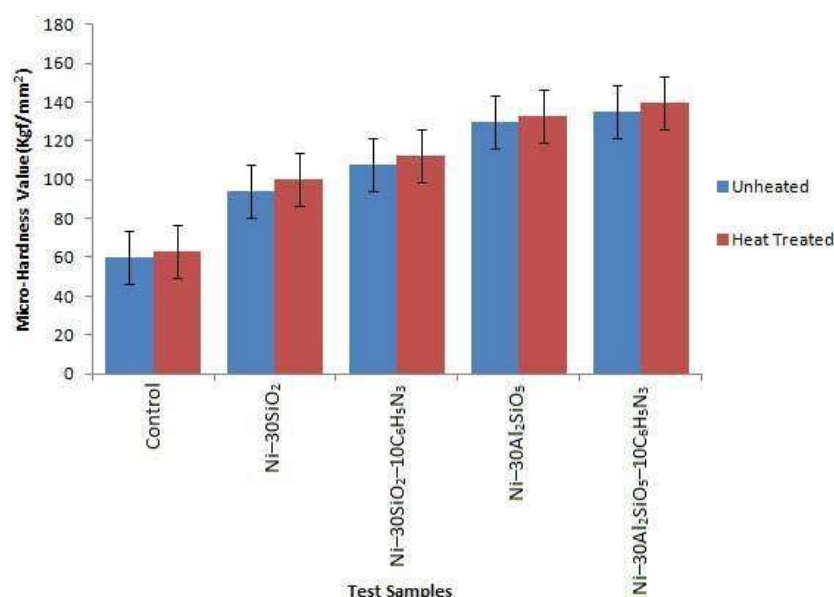
Figure 2. Micro-hardness of the heat-treated and unheated samples.

These values were obtained using the Vickers hardness technique, with the aid of high diamond pyramid indentation (EMCO Test Dura-scan), at a test load of 10 g, for 20 s.

Indentations were carried out across the mild steel samples surfaces, at an interval of 20 μm. Vickers micro hardness values were computed using the applied load, and the average diagonal of the impression created on the test samples. The micro-hardness of all the samples increased after the heat-treatment, which shows that it improved the particles adhesion kinetics [27]. Considering the unheated samples, the uncoated mild steel micro-hardness was raised from 60 to 94 kgf/mm^2, with 30g SiO_2, and further increased to 108 kgf/mm^2, with 10g $C_6H_5N_3$ particles. A similar increase was noticed with Ni–$30Al_2SiO_5$ and Ni–$30Al_2SiO_5$–$10C_6H_5N_3$ coated samples. The increment in micro-hardness could be attributed to the increase in the stain energy of the matrix alloy, as a result of the particles addition [28].

Samples wear behavior

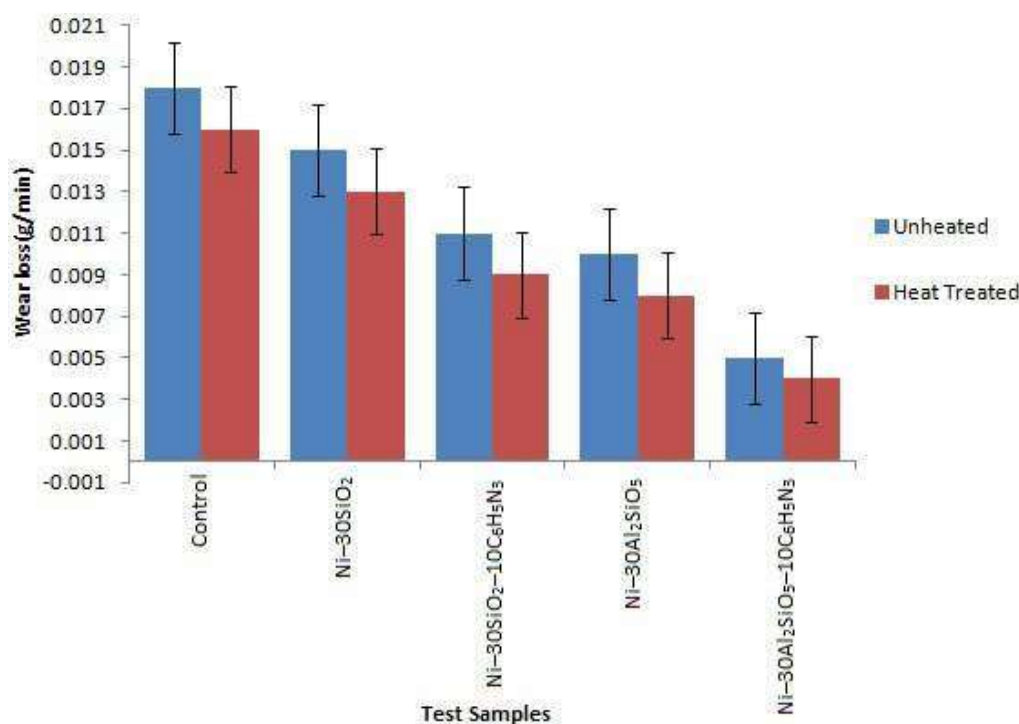Fig. 3 shows the comparative test samples wear loss.

Figure 3. Variation of the wear loss of the heat-treated and unheated samples.

The uncoated sample exhibited lower wear resistance than that of the coated sample, because the intermolecular bonds within the mild steel were easily distorted, resulting in the material wearing at a faster rate [16]. The wear resistance was found to increase after the heat-treatment. The coated sample higher wear resistance indicates that the particulates acted as a load bearing component and building block against the counter body. Ni–$30Al_2SiO_5$– $10C_6H_5N_3$ and Ni–

$30Al_2SiO_5$ coated samples suffered lower wear loss than that of the other samples, which could result from the load bearing capacity of the hard Al_2SiO_5 and from the good bonding between the particles and the matrix.

This, consequently, minimizes the particles pull out. More so, the coating mass particles concentration, size and homogenous distribution could have increased the anti-wear action that results from the elemental stability between mild steel and Al_2SiO_5 [8, 11].

Morphology of the unheated and heat-treated samples

Figs. 4a-e shows the high resolution optical microscopy micrographs of the unheated coated and uncoated samples.
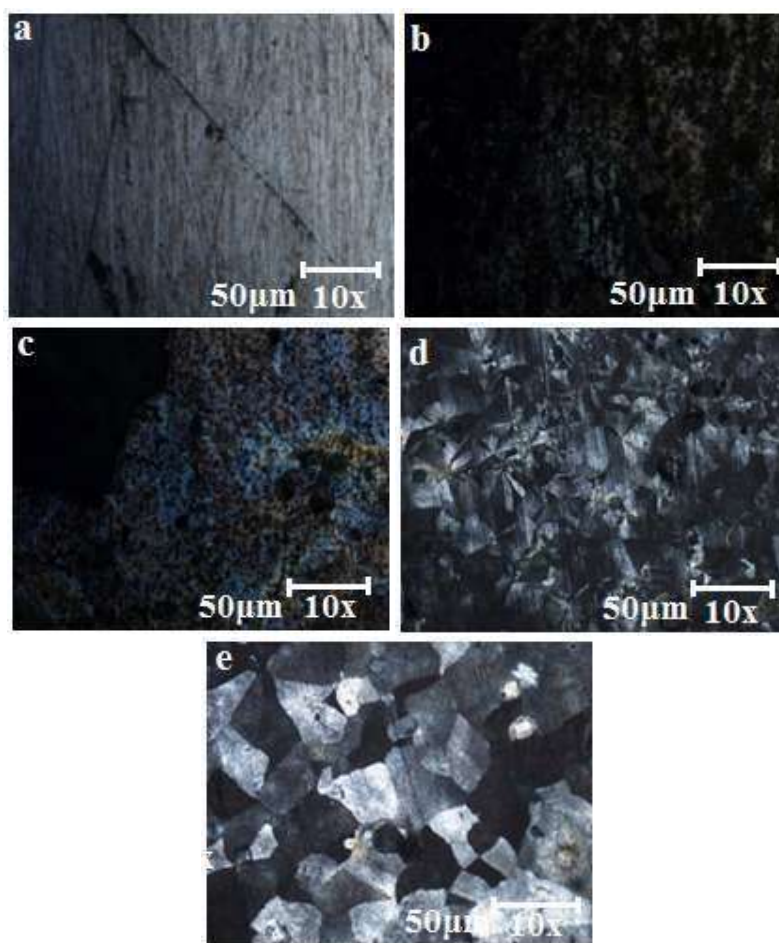

Figure 4. Micrographs of mild steel: (a) uncoated; (b) Ni–$30SiO_2$ coated; (c) Ni–$30SiO_2$–$10C_6H_5N_3$ coated; (d) Ni–$30Al_2SiO_5$ coated and; (e) Ni–$30Al_2SiO_5$–$10C_6H_5N_3$ coated.

Expectedly, the micrograph of the uncoated mild steel surface exhibited rough morphology and initiation of pitting corrosion [29, 30]. Fig. 4b-e shows the growth of several crystals on the mild steel surface, without defects and minimal porosity. Figs. 4b and 4c appear darker and smoother, signifying the presence of similar particles in the coated samples. However, Figs. 4d and 4e exhibit a unique flakelike crystalline structure at the mild steel surface. This could be linked to the Al_2SiO_5 nanoparticles inclusion and uniform dispersion in the Ni matrix, which resulted in the generation of more nucleation sites, and minimized the crystal growth, leading

to the development of nano-sized grains [31-33]. The synergy between Al_2SiO_5 and the whitish $C_6H_5N_3$ could have been the reason for the double phases displayed by the micrograph in Fig. 4e, which represents the Ni– $30Al_2SiO_5–10C_6H_5N_3$ coated sample [34]. However, it possesses a brighter and smoother morphology than that of the other samples.

The high resolution optical microscopy micrographs of the heat-treated samples are shown in Figs. 5a-e.
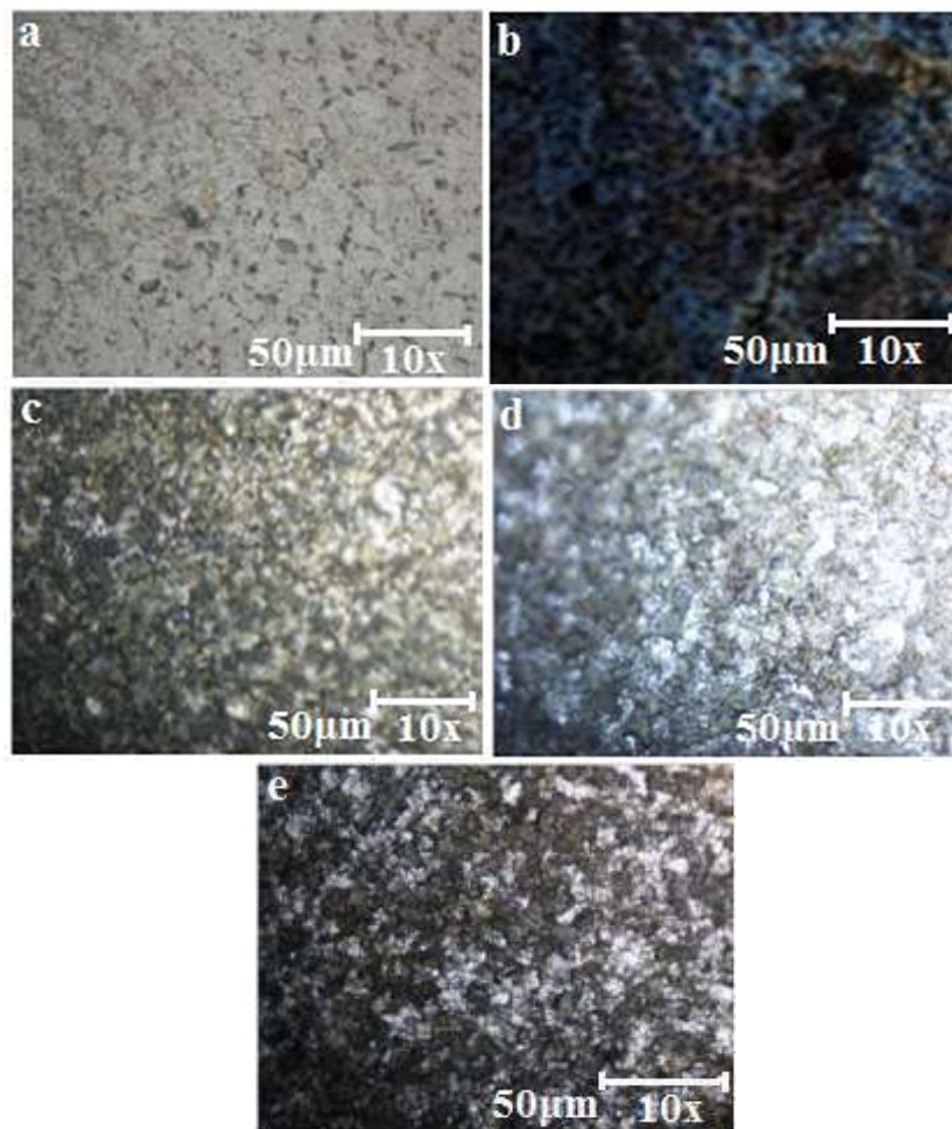

Figure 5. Micrographs of heat-treated mild steel: **(a)** uncoated; **(b)** Ni–$30SiO_2$ coated; **(c)** Ni–$30SiO_2–10C_6H_5N_3$ coated; **(d)** Ni–$30Al_2SiO_5$ coated and; **(e)** Ni–$30Al_2SiO_5–10C_6H_5N_3$ coated.

The micrograph of the heat-treated mild steel shown in Fig. 5a appears rougher than that of the mild steel in Fig. 4a. Little cracks were also noticed on the micrograph. This crack formation could result from the iron oxide (Fe_2O_3) growth, when it was treat-heated to 400 °C, for 1 h [35]. Although, due to the oxide formation, a change in color was observed in the micrograph of Figs. 5b-e, compared to those of the unheated samples in Figs. 4b-e coatings, with a

continuous and crack-free morphology. This achievement could be ascribed to the particles surface refinement behavior, and to the coated steel oxidation kinetics [36]. In Figs. 5c and 5e, the coating matrix modification, as a result of the $C_6H_5N_3$ addition, might have delayed the oxidation process, and, consequently, reduced the stress in the coating matrix. More so, the oxide films could have been responsible for the enhanced substrate oxidation resistance [37].

Conclusions

The electrodeposition of Ni–$30SiO_2$, Ni–$30SiO_2$–$10C_6H_5N_3$, Ni–$30Al_2SiO_5$ and Ni–$30Al_2SiO_5$–$10C_6H_5N_3$ coatings on mild steel was achieved. The modified mild steel exhibited better strengthening characteristics than those of the uncoated steel, due to the coatings adhesion onto the substrate. Improved corrosion and wear resistance were also observed for all the coated samples. The Ni–$30Al_2SiO_5$–$10C_6H_5N_3$ coated steel exhibited the lowest wear loss, and also offered the highest resistance to the attack by the corrosive agents. The coated mild steel good surface morphology indicated that the particles were well dispersed during the electrodeposition process, which impacted on its electrochemical behavior, micro-hardness characteristics and wear resisting capacity. Comparatively, Ni–$30Al_2SiO_5$–$10C_6H_5N_3$ coated mild steel exhibited the overall best performance characteristics.

Acknowledgments

Authors' contribution

I. G. Akande: performed the analysis – analyzed data; wrote the paper – developed some sections of the manuscript. **O. S. I. Fayomi**: conceived and designed the analysis – conceptualized ideas; offered key intellectual support, assessed and appraised the manuscript; wrote the paper – developed some sections of the manuscript. **A. P. I. Popoola**: conceived and designed the analysis: conceptualized ideas; offered key intellectual support, assessed and appraised the manuscript. **T. Daantjie**: performed the analysis – performed the experiment and analyzed data; wrote the paper – developed some sections of the manuscript. **O. O. Oluwole**: offered key intellectual support, assessed, reviewed and appraised the manuscript. **B. O. Olatunji**: assisted in the plagiarism test and edition of the manuscript.

References

1. Praveen BM, Venkatesha TV. Electrodeposition and properties of Znnanosized TiO_2 composite coatings. Appl Surf Sci. 2008;254(8):2418-24. DOI: https://doi.org/10.1016/j.apsusc.2007.09.047
2. Akande IG, Fayomi OSI, Oluwole OO. Performance of composite coating on carbon steel–A Necessity. Energy Procedia. 2019;157:375-383. DOI: https://doi.org/10.1016/j.egypro.2018.11.202
3. Ayoola AA, Fayomi OSI, Akande IG, et al. Inhibitive Corrosion Performance of the Eco-Friendly Aloe Vera in Acidic Media of Mild and Stainless Steels. J

Bio Tribo-Corros. 2020;6:1-13. DOI: https://doi.org/10.1007/s40735-02000361-y

4. Pancrecious JK, Ulaeto SB, Ramya R, et al. Metallic composite coatings by electroless technique–a critical review. Int Mat Rev. 2018;63(8):488-512. DOI: https://doi.org/10.1080/09506608.2018.1506692

5. Fayomi OSI, Sode A, Akande IG, et al. Improving the structural properties and corrosion behavior of electroless deposited Ni-P-Zn coatings on mild steel for advanced processes. AIMS Mat Sci. 2020;7:441-452. DOI: https://doi.org/10.3934/matersci.2020.4.441

6. Abou-Krisha MM, Assaf FH, El-Naby SA. Electrodeposition behavior of zinc–nickel–iron alloys from sulfate bath. J Coat Technol Res. 2009;6(3):391-399. DOI: https://doi.org/10.1007/s11998-008-9134-4

7. Roventi G, Cecchini R, Fabrizi A, et al. Electrodeposition of nickel–zinc alloy coatings with high nickel content. Surf Coat Technol. 2015;276:1-7. DOI: https://doi.org/10.1016/j.surfcoat.2015.06.043

8. Ruidong XU, Junli WA, Zhongcheng GU, et al. Effects of rare earth on microstructures and properties of Ni-WP-CeO2-SiO2 nano-composite coatings. J Rare Earths. 2008;26(4):579-583. DOI: https://doi.org/10.1016/S1002-0721(08)60141-6

9. Monyai T, Fayomi OS, Popoola AP, et al. Integration of MoO_2 composite on the micro-evolution and anticorrosion mitigation of $Zn–Ni–MoO_2$ thin films coating by electrodeposition system. J Bio Tribo-Corros. 2019;1:1-9. DOI: https://doi.org/10.1007/s40735-018-0206-4

10. Wang TG, Jeong D, Liu Y, et al. Study on nanocrystalline Cr2O3 films deposited by arc ion plating: II. Mechanical and tribological properties. Surf Coat Technol. 2012;206(10):2638-2644. DOI: https://doi.org/10.1016/j.surfcoat.2011.10.026

11. Hammami O, Dhouibi L, Bercot P, et al. Effect of phosphorus doping on some properties of electroplated Zn–Ni alloy coatings. Surf Coat Technol. 2013;219:119-125. DOI: https://doi.org/10.1016/j.surfcoat.2013.01.014

12. Shibli SM, Chacko F, Divya C. $Al_2O_3–ZrO_2$ mixed oxide composite incorporated aluminum rich zinc coatings for high wear resistance. Corros Sci. 2010;52(2):518-525. DOI : https://doi.org/10.1016/j.corsci.2009.10.008

13. Paturi UM, Cheruku S, Geereddy SR. Process modeling and parameter optimization of surface coatings using artificial neural networks (ANNs): State-of-the-art review. Mat Today: Proceed. 2021;38:2764-2774. DOI: https://doi.org/10.1016/j.matpr.2020.08.695

14. Aal AA, Barakat MA, Mohamed RM. Electrophoreted Zn–TiO2–ZnO nanocomposite coating films for photocatalytic degradation of 2chlorophenol. Appl Surf Sci. 2008;254(15):4577-4583. DOI: https://doi.org/10.1016/j.apsusc.2008.01.049

15. Su YL, Kao WH. Tribological behaviour and wear mechanism of $MoS_2–Cr$ coatings sliding against various counterbody. Tribol Int. 2003;36(1):11-23. DOI: https://doi.org/10.1016/S0301-679X(02)00095-6

16. Dong D, Chen XH, Xiao WT, et al. Preparation and properties of electroless $Ni–P–SiO_2$ composite coatings. Appl Surf Sci. 2009;255(15):7051-7055. DOI: https://doi.org/10.1016/j.apsusc.2009.03.039

17. Walsh FC, Wang S, Zhou N. The electrodeposition of composite coatings: Diversity, applications and challenges. Current Opin Electrochem. 2020;20:8-19. DOI : https://doi.org/10.1016/j.coelec.2020.01.011

18. Subramanian B, Mohan S, Jayakrishnan S. Structural, microstructural and corrosion properties of brush plated copper–tin alloy coatings. Surf Coat Technol. 2006;201(3-4):1145-1151. DOI: https://doi.org/10.1016/j.surfcoat.2006.01.042

19. Frade T, Bouzon V, Gomes A, et al. Pulsed-reverse current electrodeposition of Zn and Zn-TiO2 nanocomposite films. Surf Coat Technol. 2010;204(2122):3592-3598. DOI: https://doi.org/10.1016/j.surfcoat.2010.04.030

20. Arici M, Nazir H, Aksu ML. Investigation of Sn–Zn electrodeposition from acidic bath on EQCM. J Alloys Compds. 2011;509(5):1534-1537. DOI: https://doi.org/10.1016/j.jallcom.2010.10.161

21. Akande IG, Fajobi MA, Odunlami OA, et al. Exploitation of composite materials as vibration isolator and damper in machine tools and other mechanical systems: A review. Mat Today: Proceed. 2021;43:1465-1470. DOI: https://doi.org/10.1016/j.matpr.2020.09.300

22. Dong Z, Peng X, Guan Y, et al. Optimization of composition and structure of electrodeposited Ni–Cr composites for increasing the oxidation resistance. Corros Sci. 2012;62:147-152. DOI: https://doi.org/10.1016/j.corsci.2012.05.010

23. Hu YJ, Xiong L, Meng JL. Electron microscopic study on interfacial characterization of electroless Ni–W–P plating on aluminum alloy. Appl Surf Sci. 2007;253(11):5029-5034. DOI: https://doi.org/10.1016/j.apsusc.2006.11.009

24. Daniyan AA, Umoru LE, Fayomi OS. Structural evolution, optoelectrical and corrosion properties of electrodeposited WO_3 integration on $Zn-TiO_2$ electrolyte for defence super application. Defense Technol. 2018;14(5):396402. DOI: https://doi.org/10.1016/j.dt.2018.06.015

25. Low CT, Wills RG, Walsh FC. Electrodeposition of composite coatings containing nanoparticles in a metal deposit. Surf Coat Technol. 2006:12;201(1-2):371-383. DOI: https://doi.org/10.1016/j.surfcoat.2005.11.123

26. Fayomi OSI, Oluwadare GA, Fakehinde OB, et al. Evolution of physical and mechanical characteristics of deposited composite coatings on A356 mild steel. Int J Adv Manufact Technol. 2019;103(5-8):2621-2625. DOI: https://doi.org/10.1007/s00170-019-03714-1

27. Rahman MJ, Sen SR, Moniruzzaman M, et al. Morphology and properties of electrodeposited Zn-Ni alloy coatings on mild steel. J Mechan Eng. 2009;40(1):9-14. DOI: https://doi.org/10.3329/jme.v40i1.3468

28. Lin YC, Luo SC, Huang J, et al. Effects of solution treatment on microstructures and micro-hardness of a Sr-modified Al-Si-Mg alloy. Mat Sci Eng: A. 2018;725:530-40. DOI: https://doi.org/10.1016/j.msea.2018.04.049

29. El Wanees SA, Radwan AB, Alsharif MA, et al. Initiation and inhibition of pitting corrosion on reinforcing steel under natural corrosion conditions. Mat Chem Phys. 2017;190:79-95. DOI: https://doi.org/10.1016/j.matchemphys.2016.12.048

30. Xiang Y, Li C, Hesitao W, et al. Understanding the pitting corrosion mechanism of pipeline steel in an impure supercritical CO2 environment. J Supercrit Fluids. 2018;138:132-142. DOI: https://doi.org/10.1016/j.supflu.2018.04.009

31. Malatji N, Popoola AP, Fayomi OS, et al. Multifaceted incorporation of ZnAl$_2$O$_3$/Cr$_2$O$_3$/SiO$_2$ nanocomposite coatings: anti-corrosion, tribological, and thermal stability. Int J Adv Manufact Technol. 2016;82(5-8):1335-1341. DOI: https://doi.org/10.1007/s00170-015-7463-x

32. Anawe PA, Raji O, Fayomi OSI, et al. Influence of Composite Nano Coating on Ternary Sulphate Co-deposition: Corrosion and Surface Characterization. Procedia Manufact. 2017;7:556-561. DOI: https://doi.org/10.1016/j.promfg.2016.12.073

33. Akande IG, Oluwole OO, Fayomi OSI. Optimizing the defensive characteristics of mild steel via the electrodeposition of Zn-Si3N4 reinforcing particles. Defense Technol. 2018;15:526-532. DOI: https://doi.org/10.1016/j.dt.2018.11.001

34. Ashassi-Sorkhabi H, Rafizadeh SH. Effect of coating time and heat treatment on structures and corrosion characteristics of electroless Ni–P alloy deposits. Surf Coat Technol. 2004;176(3):318-326. DOI: https://doi.org/10.1016/S0257-8972(03)00746-1

35. Li H, Liang K, Mei L, et al. Oxidation resistance of mild steel by zirconia sol–gel coatings. Mat Sci Eng: A. 2003;341(1-2):87-90. DOI: https://doi.org/10.1016/S0921-5093(02)00200-9

36. Garcia-Heras M, Jimenez-Morales A, Casal B, et al. Preparation and electrochemical study of cerium–silica sol–gel thin films. J Alloys Cmpds. 2004;380(1-2):219-224. DOI: https://doi.org/10.1016/j.jallcom.2004.03.047

37. Phanasgaonkar A, Raja VS. Influence of curing temperature, silica nanoparticles and cerium on surface morphology and corrosion behavior of hybrid silane coatings on mild steel. Surf Coat Technol. 2009;203(16):2260-2271. DOI: https://doi.org/10.1016/j.surfcoat.2009.02.020